An Ensemble Approach to Investigate Tropical Cyclone Intensification in Sheared Environments. Part II: Ophelia (2011)

ROSIMAR RIOS-BERRIOS AND RYAN D. TORN

Department of Atmospheric and Environmental Sciences, University at Albany, State University of New York, Albany, New York

CHRISTOPHER A. DAVIS

National Center for Atmospheric Research, Boulder, Colorado*

(Manuscript received 18 August 2015, in final form 3 December 2015)

ABSTRACT

The mechanisms leading to tropical cyclone (TC) intensification amid moderate vertical wind shear can vary from case to case, depending on the vortex structure and the large-scale conditions. To search for similarities between cases, this second part investigates the rapid intensification of Hurricane Ophelia (2011) in an environment characterized by 200–850-hPa westerly shear exceeding $8\,m\,s^{-1}$. Similar to Part I, a 96-member ensemble was employed to compare a subset of members that predicted Ophelia would intensify with another subset that predicted Ophelia would weaken. This comparison revealed that the intensification of Ophelia was aided by enhanced convection and midtropospheric moisture in the downshear and left-of-shear quadrants. Enhanced left-of-shear convection was key to the establishment of an anticyclonic divergent outflow that forced a nearby upper-tropospheric trough to wrap around Ophelia. A vorticity budget showed that deep convection also contributed to the enhancement of vorticity within the inner core of Ophelia via vortex stretching and tilting of horizontal vorticity enhanced by the upper-tropospheric trough. These results suggest that TC intensity changes in sheared environments and in the presence of upper-tropospheric troughs highly depend on the interaction between convective-scale processes and the large-scale flow. Given the similarities between Part I and this part, the results suggest that observations from the three-dimensional moisture and wind fields could improve both forecasting and understanding of TC intensification in moderately sheared environments.

1. Introduction

a. Review of Part I

In Rios-Berrios et al. (2016, hereafter Part I), we investigated the intensity changes of Katia, a weak tropical storm that intensified in spite of moderate easterly vertical wind shear between 200 and 850 hPa. Intensity forecasts produced with a 96-member ensemble were used to compare scenarios where Katia intensified with scenarios where Katia remained a weak tropical storm. It was found that intensification was aided by enhanced lower-tropospheric moisture that supported buoyant updrafts near the center of Katia. As the updrafts became deeper and stronger, midtropospheric moisture increased and supported sustained deep convection. A vorticity budget revealed that the circulation of Katia increased locally owing to vortex stretching and tilting of the horizontal vorticity by convective updrafts. These findings share similarities with the pathway proposed by Dolling and Barnes (2012) in which enhanced instability, buoyant updrafts, and vortex stretching drive the gradual intensification of tropical storms.

This second part will verify the robustness of those results by considering Hurricane Ophelia (2011), which rapidly intensified from a weak tropical storm to a category-4 hurricane in the presence of 200–850-hPa westerly vertical shear magnitudes in excess of $8\,m\,s^{-1}$ (Fig. 1). Contrary to the wind profile surrounding

* The National Center for Atmospheric Research is sponsored by the National Science Foundation.

Corresponding author address: Rosimar Rios-Berrios, University at Albany, State University of New York, DAES-ES 325, 1400 Washington Ave., Albany, NY 12222.
E-mail: rrios-berrios@albany.edu

DOI: 10.1175/JAS-D-15-0245.1

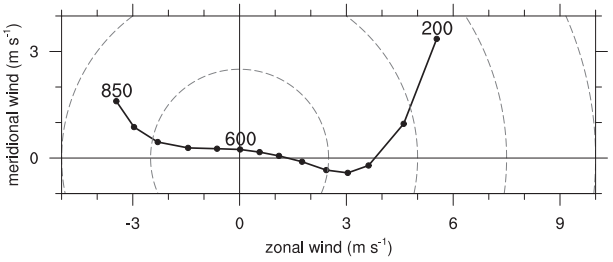

FIG. 1. Composite hodograph from the 96-member AHW ensemble forecasts initialized at 1200 UTC 28 Sep 2011. Dots represent area-averaged winds within a 500-km radius of Ophelia from 850 to 200 hPa every 50 hPa.

Katia, the wind profile around Ophelia was characterized by a large vertical gradient between 600 and 200 hPa due to the presence of an upper-tropospheric trough. Given the uniqueness of this case, the following subsection provides a complementary literature review to Part I.

b. *Literature review*

Vertical wind shear tilts the tropical cyclone (TC) vortex from its upright position as result of differential vorticity advection (e.g., Raymond 1992; Jones 1995). Although this effect was not discussed in Part I, recent literature describe TC resiliency to shear as the ability of the vortex to restore its vertical alignment (Reasor et al. 2004; Reasor and Eastin 2012; Reasor and Montgomery 2015). Theoretical work predicts that large, strong, high-latitude TCs in regions of low static stability should have a faster realignment than small, weak, and low-latitude TCs in regions of high static stability (Jones 1995; DeMaria 1996; Reasor et al. 2004). Although some of these relationships have been confirmed in moist numerical simulations (Riemer et al. 2013; Reasor and Montgomery 2015), the influence of moist convection on vortex realignment is not well understood (Davis et al. 2008b). Nevertheless, recent modeling studies on TC development support that vortex realignment is key for the formation and intensification of the low-level vortex (Rappin and Nolan 2012; Ge et al. 2013; Zhang and Tao 2013; Tao and Zhang 2014). However, vortex realignment appears to be less influential when a low-level vortex has already formed because composite airborne observations show small and insignificant tilt differences between intensifying and steady state TCs (Rogers et al. 2013). Since Rogers et al. (2013) only considered hurricane-strength TCs, the role of vortex tilt might be more relevant for intensity changes of weak tropical storms.

Oftentimes a moderately sheared environment stems from an upper-tropospheric trough in close proximity to a TC (e.g., Hanley et al. 2001; Davis and Bosart 2002; Molinari et al. 2006; Shu et al. 2014). In a composite study of TC–trough interactions in the North Atlantic, Hanley et al. (2001) found that TCs are more likely to intensify than weaken after interacting with upper-tropospheric troughs. Hanley et al. (2001) explained that TC intensification was favored in situations of smaller and weaker upper-tropospheric potential vorticity (PV) disturbances than in the cases of TC weakening due to the weaker shear and stronger divergence aloft. However, the composite study of western North Pacific TCs of Shu et al. (2014) showed that upper-tropospheric troughs can inhibit intensification by promoting dry-air intrusion and reducing convective activity. Although Shu et al. (2014) restricted their study to TCs near the western North Pacific subtropical high, their results suggest that upper-tropospheric troughs could provide a mechanism for dry-air entrainment, which is a known detrimental effect of vertical wind shear (Riemer et al. 2010; Munsell et al. 2013; Tang and Emanuel 2012). These contradicting results warrant further investigation to discern the role of upper-tropospheric troughs on TC intensity changes.

This second part investigates how Ophelia rapidly intensified in the presence of moderate vertical wind shear while also exploring the interaction between Ophelia and an upper-tropospheric trough. An overview of the observed evolution of Ophelia and a brief discussion of the methods are presented in section 2. Analyses of the intensification of Ophelia are discussed in sections 3–7. General conclusions, including a comparison with Part I, are presented in section 8.

2. Synopsis of TC Ophelia (2011) and the AHW forecasts

The evolution of Ophelia was described by Avila and Stewart (2013); thus, only a summary is presented here. Ophelia formed from a vigorous African easterly wave that interacted with a low pressure system over the coastal waters of West Africa. The National Hurricane Center determined that the tropical disturbance became a tropical depression at 1800 UTC 20 September 2011. Despite gradual fluctuations in intensity between 15 and 28 m s^{-1} from 20 to 25 September, the low-level circulation of Ophelia dissipated at 1200 UTC 25 September. However, a low-level circulation was reestablished northwest of the Leeward Islands at 1200 UTC 27 September. After reforming, Ophelia intensified to tropical storm intensity at 0600 UTC 28 September. At this time, there was large uncertainty in the intensity forecasts partly as a result of moderate shear associated with an upper-level trough over the eastern United States

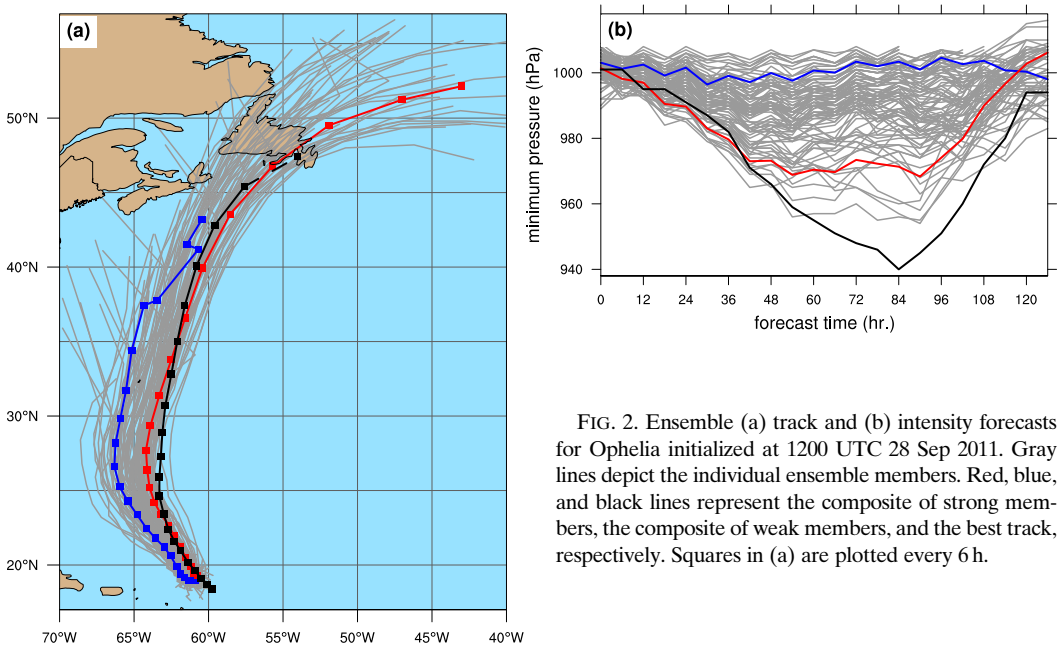

FIG. 2. Ensemble (a) track and (b) intensity forecasts for Ophelia initialized at 1200 UTC 28 Sep 2011. Gray lines depict the individual ensemble members. Red, blue, and black lines represent the composite of strong members, the composite of weak members, and the best track, respectively. Squares in (a) are plotted every 6 h.

and a subtropical ridge over the central Atlantic. Despite the shear, Ophelia intensified to hurricane strength at 1500 UTC 29 September, underwent rapid intensification afterward, and reached peak intensity of 62 m s^{-1} at 0000 UTC 2 October. Ophelia quickly weakened thereafter and transitioned into a strong extratropical cyclone.

Ensemble forecasts

High-resolution, full-physics, ensemble forecasts of Ophelia were produced with the Advanced Hurricane Weather Research and Forecasting (AHW) Model (Davis et al. 2008a, 2010). As in Part I, the main configuration of the model included three domains with 36-, 12-, and 4-km grid spacing, respectively. This configuration was used in all 96 members that were generated with a 6-hourly cycling ensemble Kalman filter (EnKF) data assimilation system, following the same methods described in Part I. As such, the initial-time perturbations are consistent with analysis errors (Cavallo et al. 2013), which depend on observation density and error growth during each assimilation cycle. The focus here will be 5-day forecasts that were initialized at 1200 UTC 28 September 2011, when Ophelia was affected by 200–850-hPa westerly shear of approximately 8 m s^{-1} (Fig. 1). Analysis errors for this initialization time are likely greater than operational analysis errors owing to the lack of in situ data near Ophelia and the fact that satellite radiance observations were not assimilated.

The AHW ensemble track and intensity forecasts generally captured the evolution of Ophelia from 1200 UTC 28 September to 0000 UTC 4 October (Fig. 2). Most of the ensemble members predicted well the observed motion of Ophelia over the western Atlantic, but the ensemble generally predicted a faster and more westward track than it was observed (Fig. 2a). The intensity forecasts captured the evolution of Ophelia as it rapidly deepened and then weakened (Fig. 2b), but all members missed the peak intensity potentially because of the relatively small radius of maximum winds (28 km). These intensity forecasts, similar to the intensity forecasts for Katia, exhibited large variability as reflected in the ensemble standard deviation, which quickly increased from 2.4 hPa at 0 h to 10.1 hPa at 84 h. A notable difference between the two cases is that the separation between intensity forecasts of Ophelia happened quickly after 0 h, whereas the ensemble forecasts of Katia had a small standard deviation (1–3 hPa) up to 48 h and quickly increased thereafter to a 16-hPa ensemble standard deviation at 126 h.

The large variability of intensity forecasts provided motivation to investigate why some members predicted intensification, while other members predicted weakening or even dissipation during the forecast period. This case could present similar or different underlying mechanisms to those identified in the case of Katia, which could be useful to understanding pathways to TC intensification in moderately sheared environments. To identify the mechanisms behind different intensity changes, two subsets of 12 members each were chosen for comparison: a subset of members with the lowest

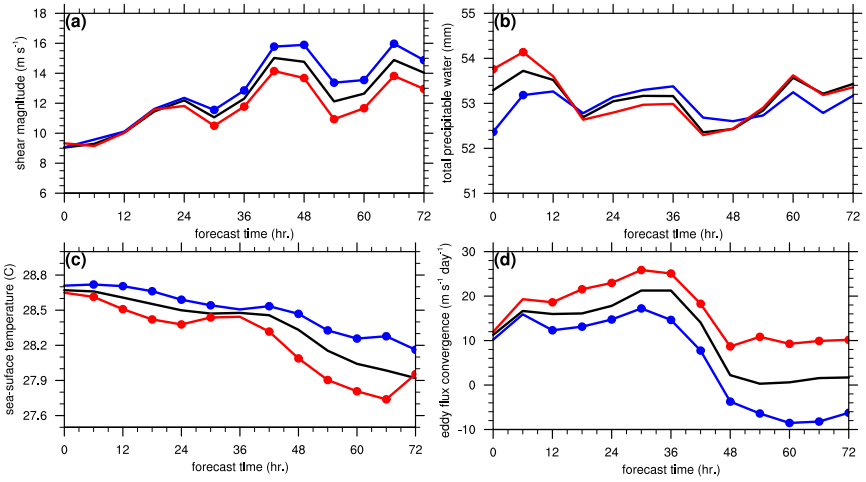

FIG. 3. Time series of (a) 200–850-hPa environmental vertical wind shear magnitude, (b) precipitable water, and (c) sea surface temperature averaged within a 500-km radius of Ophelia. Black, red, and blue lines depict the mean of the 96-member ensemble, the mean of strong members, and the mean of weak members, respectively. Dots are shown at lead times when the difference between strong and weak members is statistically significant differences at the 95% confidence level. (d) As in (a), but for the 200-hPa eddy momentum flux convergence averaged between 300 and 600 km of Ophelia.

mean 0–84 h MSLP[1] (named strong members) and a subset of members with the highest mean 0–84 h MSLP (named weak members). On average, the difference between the MSLP of these subsets was small (3 hPa) at 0 h and quickly increased to 29 hPa at 84 h (Fig. 2b). Composites of these two subsets will be compared in the following sections to understand similarities and differences among ensemble members and to test the results for statistical significance using the bootstrap resampling method introduced in Part I.

3. Diagnoses of TC Ophelia forecasts

a. Comparison of the environments

Contrary to what was found in Part I, variability in the environment appears to have little impact on the intensity forecasts of Ophelia. Strong and weak members have similar 200–850-hPa vertical shear[2] magnitudes up to 24 h (Fig. 3a) even though strong members have deepened about 10 hPa more than weak members (Fig. 2b). After 24 h, the shear magnitude is statistically significantly lower in strong members compared to weak members, but the shear of both subsets remains strong (above 10 m s^{-1}). Both subsets have similar precipitable water (PW) for most of the forecast, except between 0 and 6 h when strong members have approximately 1.5 mm more PW than weak members (Fig. 3b). The only variable that is consistently significant throughout the forecast is the sea surface temperature (SST); contrary to expectation, strong members move over cooler SSTs than weak members (Fig. 3c) because of the track differences (Fig. 2a).

Another aspect of the large-scale environment around Ophelia is the presence of an upper-tropospheric trough (Avila and Stewart 2013). The interaction between the upper-tropospheric trough and Ophelia can be quantified by means of the eddy momentum flux convergence (EFC; Molinari and Vollaro 1990; Hanley et al. 2001). The EFC is expressed as

$$\mathrm{EFC} = -\frac{1}{r^2}\frac{\partial}{\partial r}\left(r^2\overline{u_s'v_s'}\right), \tag{1}$$

where u_s represents storm-relative radial wind, v_s represents storm-relative tangential wind, r represents radius, the overbar denotes an azimuthal average, and the prime denotes a perturbation from the azimuthal average. Equation (1) is proportional to the local rate of change of azimuthally averaged tangential wind, such that an eddy source of cyclonic (anticyclonic) momentum along with storm-relative inflow (outflow) can enhance the cyclonic momentum of the TC vortex. Similar to Hanley et al. (2001), TC–trough interaction happens when the 200-hPa

[1] Only the 0–84-h forecasts were considered to exclude the period of extratropical transition in the selection of the members for each subset.

[2] Environmental shear was calculated by first removing the TC vortex using the methods of Galarneau and Davis (2013) and then taking an area average around Ophelia.

EFC exceeds $10\,m\,s^{-1}\,day^{-1}$ averaged between a radius of 300 and 600 km from the TC.

As shown in Fig. 3d, both strong and weak members have an EFC greater than $10\,m\,s^{-1}\,day^{-1}$ during the first 30 h, which confirms that a TC–trough interaction is taking place. The EFC of strong members is 5–$10\,m\,s^{-1}\,day^{-1}$ significantly greater than the EFC of weak members at and beyond 12 h, but no significant differences appear at 0 and 6 h. The lack of significant differences during a period when strong members are already intensifying suggests that other factors must initiate the intensification of Ophelia in strong members but inhibit intensification in weak members. Once that initial intensification takes place, the stronger EFC could allow strong members to continue their intensifying trend, as will be shown later.

b. Storm-relative differences

Given the rapid separation between strong and weak members, the 0- and 6-h significant PW differences deserve further investigation. Strong members have greater environmental PW during that period, which could set the stage for greater convective activity in strong members. However, convective activity around sheared storms is asymmetrically distributed such that updrafts are initiated to the right of the shear vector, deepened to the left of the shear vector, and replaced by downdrafts in the upshear quadrant (Reasor et al. 2013; DeHart et al. 2014). Since the environmental PW was both vertically and horizontally integrated, that metric does not indicate the location of greater moisture with respect to convection initiation. Instead, a storm-centered[3] comparison between strong and weak members is employed to determine the location and timing of moisture variability around Ophelia.

As evidenced by Figs. 4a–c, moisture differences between strong and weak members are not symmetrically distributed around Ophelia at 0 h. The PW of strong members is 1.6 standard deviations (σ) greater than the PW of weak members to the east-northeast (downshear) of Ophelia (Fig. 4a). A sharp gradient exists over that region in the ensemble mean; thus, the differences relate to variability in the radial extent of moisture around Ophelia. Evaluating the water vapor mixing ratio at different levels reveals that the largest water vapor differences at 0 h exist mostly in the middle troposphere (Figs. 4b,c). While the differences in 950-hPa water vapor mixing ratio are small and sporadically located around Ophelia, the 500-hPa water vapor mixing ratio is 1.6σ greater in strong members within the same region of significant PW differences. Strong members additionally have stronger 500-hPa tangential winds collocated with greater 500-hPa water vapor than weak members (Fig. 7c), which could result in greater moisture advection cyclonically around Ophelia (to be shown later).

By 12 h, strong members have 0.8–2.0σ more PW within 2° north of Ophelia but 0.8–1.6σ less PW to the south and west of Ophelia (Fig. 4d). Taking an area average of positive and negative differences can result in a small value, which is why no significant differences appeared in the environmental diagnostic of PW. Within the region of positive PW differences, strong members have 0.8–1.6σ smaller 950-hPa water vapor mixing ratio (Fig. 4e) but over 2.0σ larger 500-hPa water vapor mixing ratio than weak members (Fig. 4f). This result implies that strong members have more convection, as will be shown later, accompanied by drier air that spreads away from Ophelia in the lower troposphere. Strong members also have greater 950-hPa water vapor mixing ratio within a narrow band south and west (right of shear and downshear) of Ophelia that can serve as a region of greater convective initiation.

Moisture differences between strong and weak members continue to be asymmetrically distributed by 24 h (Figs. 4g–i). Strong members have 2.5σ more PW within 2° of Ophelia, but the largest PW differences have rotated cyclonically to the west (upshear) of Ophelia (Fig. 4g). Radially outward of the positive PW differences, strong members have between 0.8 and 1.2σ smaller 950-hPa water vapor mixing ratio than weak members (Fig. 4h). As a result of this drier air, strong members have a greater moisture disequilibrium resulting in up to 2.5σ stronger surface moisture fluxes to the west (upshear) of the TC center (not shown). Cyclonically upwind of the drier air and stronger fluxes, strong members have 0.8–1.2σ greater 950-hPa water vapor mixing ratio within a banding feature that wraps around and into the center of Ophelia. Strong members also have up to 2.0σ greater 500-hPa mixing ratio primarily to the west (upshear) of Ophelia (Fig. 4i). These midtropospheric differences continue amplifying in magnitude and coverage beyond 24 h while the drier air remains well away from the inner-core circulation (not shown).

4. Analysis of water vapor differences

Storm-relative water vapor differences highlight the asymmetric nature of near-storm moisture differences around Ophelia; strong members have more midtropospheric moisture in the downshear quadrant at

[3] As in Part I, the storm-centered analysis is based on the 850-hPa vortex center of Ophelia.

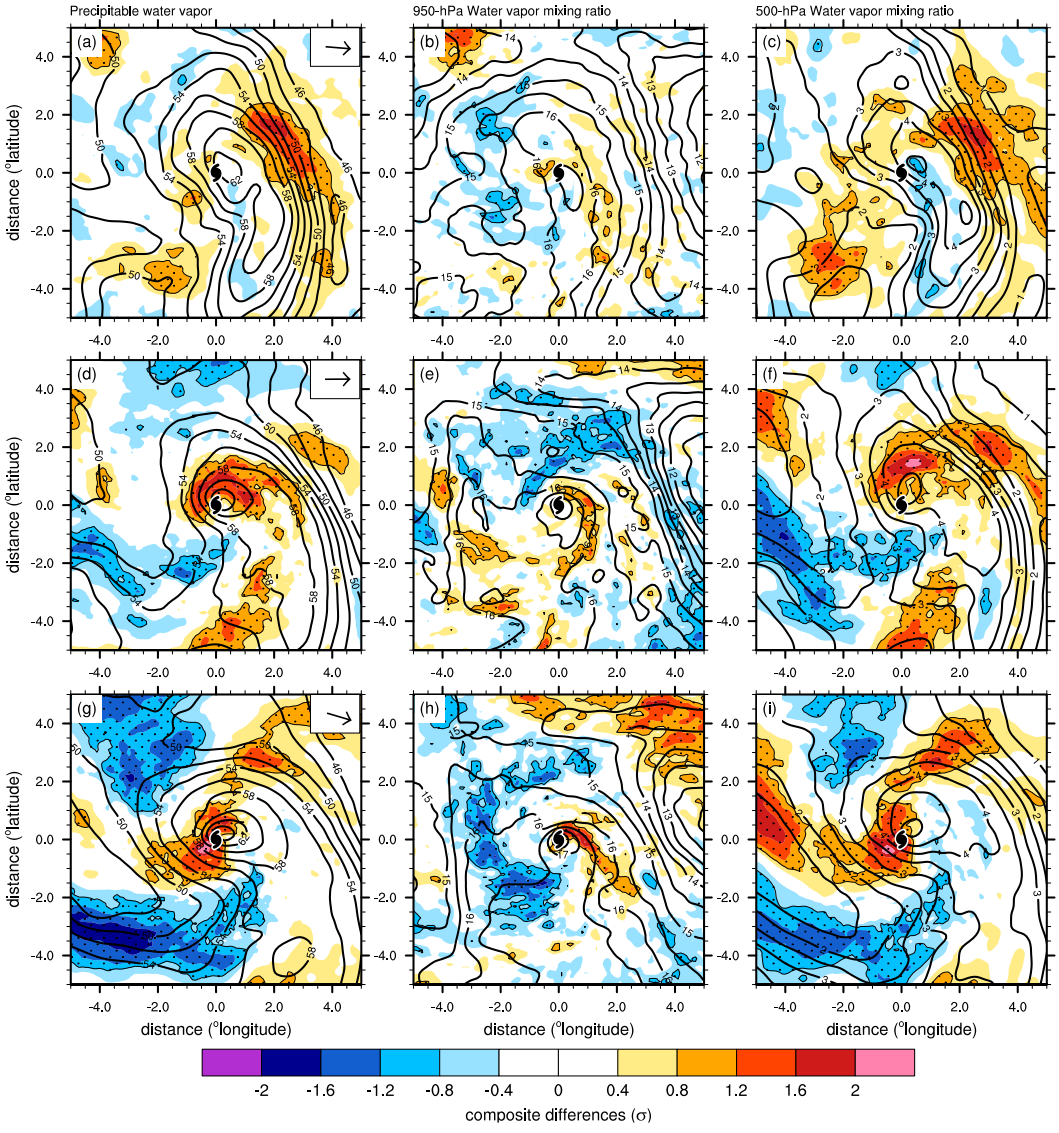

FIG. 4. Latitude–longitude analysis of storm-centered composites relative to the 850-hPa vortex center of each ensemble member at (a)–(c) 0, (d)–(f) 12, and (g)–(i) 24 h. Panels show the standardized composite differences between the mean of strong members and the mean of weak members (shading, every 0.4σ) of (a),(d),(g) precipitable water, (b),(e),(h) 950-hPa water vapor mixing ratio, and (c),(f),(i) 500-hPa water vapor mixing ratio. The ensemble mean of each quantity is shown by the black contour lines [(a),(d),(g) every 2 mm, (b),(e),(h) every 1 g kg^{-1}, and (c),(f),(i) every 0.5 g kg^{-1}]. Statistically significant differences are denoted by the stippling pattern. The 200–850-hPa shear vector is depicted by the arrow in (a), (d), and (g).

0 h, in the left-of-shear quadrant at 12 h, and in the upshear quadrant at 24 h. This propagation of water vapor differences around the TC was also noted in Part I, but in that case strong members initially had more lower-tropospheric moisture and eventually gained more midtropospheric moisture by the action of buoyant updrafts. To elucidate this discrepancy between the two cases and identify the source of greater moisture in strong members, backward parcel trajectories were computed for approximately 110 parcels that end within the 500-hPa moisture differences north of Ophelia at 12 h (cf. Fig. 4f). Parcel trajectories were integrated backward in time to 0 h using the Read/Interpolate/Plot[4] (RIP) software with 6-min output from the 4-km domain of one member from each subset.

[4] The Read/Interpolate/Plot software can be accessed at http://www2.mmm.ucar.edu/wrf/users/docs/ripug.htm.

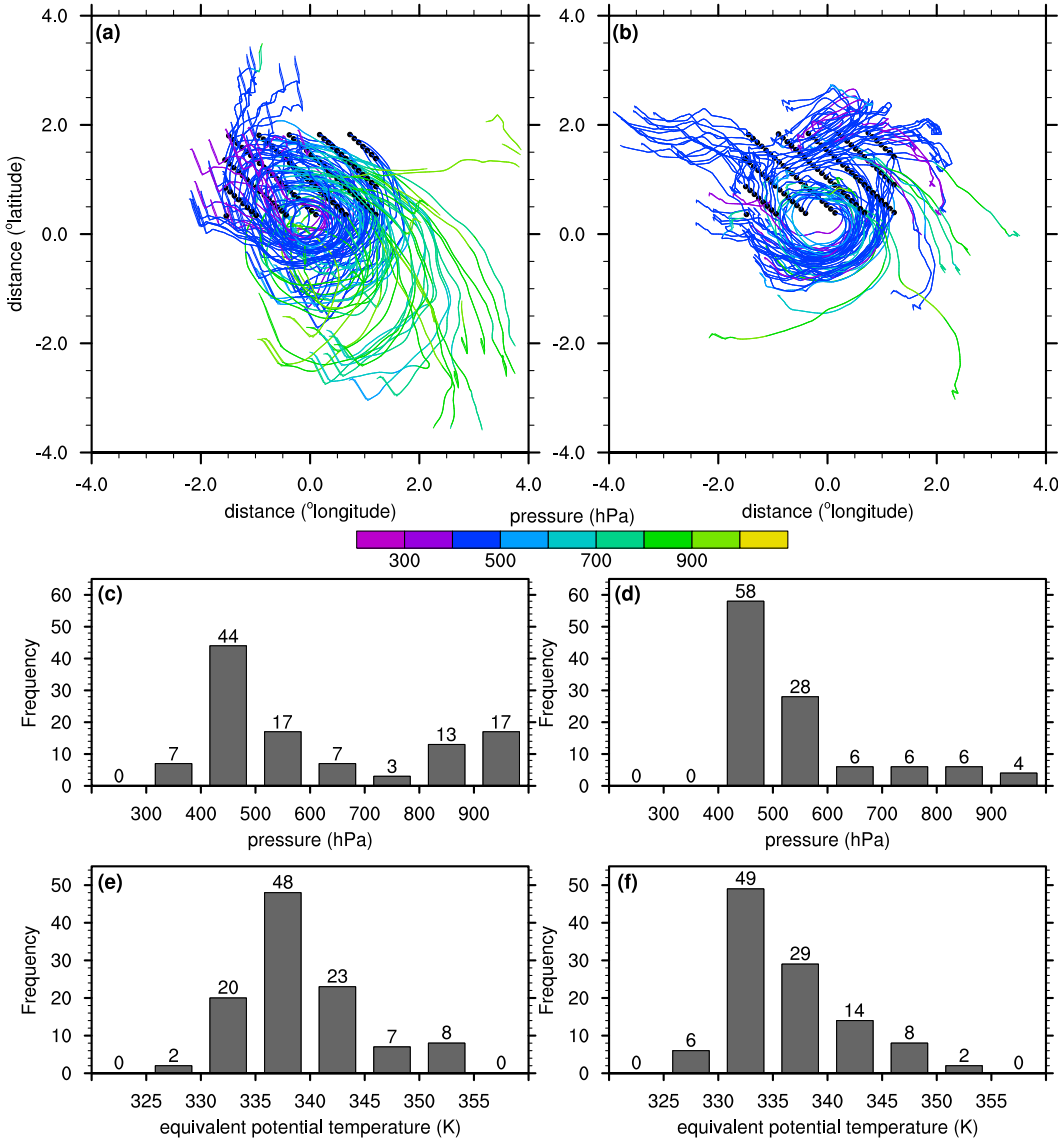

FIG. 5. Backward trajectory analysis of parcels released from the 500-hPa level north of Ophelia at 12 h. Analysis for a (left) strong and (right) weak member. (a),(b) Color shading represents pressure along the trajectories and black dots represent the location of the parcels at 12 h. Histograms of (c),(d) pressure and (e),(f) equivalent potential temperature at the 0-h parcel location.

Despite the similar final location (i.e., at the 12-h forecast) of the parcels, backward trajectories are substantially different between the two members (Fig. 5). The backward trajectories of a strong member show two main regions where parcels originate: southeast (right of shear) and northwest (upshear) of Ophelia (Fig. 5a). Parcels originating to the southeast are generally located in the lower troposphere, between 700 and 1000 hPa, before ascending and traveling cyclonically around Ophelia. Some of these parcels begin ascending within the region where strong members have greater 950-hPa water vapor (cf. Fig. 4e). Parcels originating to the northwest, however, are mostly located above 500 hPa before descending and traveling cyclonically around Ophelia. In contrast, the backward trajectories of a weak member show most parcels originating north of Ophelia (Fig. 5b). The majority of tracked parcels travel around the surface center of circulation without substantial vertical displacement, except for some parcels that descend from the upper troposphere to 500 hPa (Fig. 5b).

To further illustrate the different properties of the parcels that ultimately end north (left of shear) of

Ophelia, distributions of pressure and equivalent potential temperature θ_e at the initial[5] location of the parcels are shown in Figs. 5c–f. The distributions of initial pressure show that 40 parcels originate between 600 and 1000 hPa in the strong member (Fig. 5c), as opposed to 22 parcels in the weak member. This difference indicates the presence of more updrafts and less downdrafts in the strong member, which is also supported by the distributions of initial θ_e. Nearly 88 parcels of the strong member have θ_e exceeding 335 K, in comparison to 53 parcels of the weak member (Figs. 5e,f). Although these values can change along the trajectories, parcels with relatively higher θ_e in the lower troposphere eventually ascend and bring significantly greater midtropospheric moisture north of Ophelia.

Figures 5a,b also show that while most of the descent occurs in the upshear side of the strong member, most of the descent occurs to the left of the shear in the weak member. The location of the region of broad descent can be linked to the tilt of the vortex, as shown by Jones (1995). When a vortex is tilted by environmental shear, the initial balanced response consists of adiabatic ascent downtilt and adiabatic descent uptilt. After an adjustment period, this response rotates anticyclonically and results in ascent to the right of the tilt and descent to the left of the tilt [cf. Fig. 5 of Jones (1995)]. This adjustment period was likely completed before the time period considered here because Ophelia reformed and was exposed to moderate shear for 24 h before the initialization of the AHW forecasts. To assess the relationship between the tilt configuration and the vertical motion patterns noted in the parcel trajectories, the lower-tropospheric (850 hPa) and midtropospheric (500 hPa) centers of circulation were identified using the following vorticity centroid method:

$$\mathbf{x}_c = \frac{\int\int \zeta \mathbf{x}\, dx\, dy}{\int\int \zeta\, dx\, dy},$$

where $\mathbf{x}_c$ is a position vector of the center of circulation, $\mathbf{x}$ is a position vector of each grid point, and ζ is relative vorticity. Integration was done within a 150-km radius from each grid point.

Figure 6 shows the 500–850-hPa tilt magnitude and tilt angle (0° represents eastward tilt) for the same individual strong and weak members used for the parcel trajectory analysis. The strong member has an initial tilt of 90 km to the north (left of shear) of Ophelia, whereas the weak member has a smaller tilt of 35 km to the east (downshear) of Ophelia. As shown in Fig. 7, these different tilt configurations are related to differences in the initial vortex structure. Strong members have a lower-tropospheric circulation that is between 0.8 and 1.2σ stronger to the southeast of Ophelia (Fig. 7a) and a midtropospheric circulation that is up to 2.0σ stronger to the north of Ophelia (Fig. 7b). The midtropospheric difference indicates that strong members have a broader midlevel circulation than weak members, which is confirmed by the 2.0σ significantly stronger 500-hPa tangential winds between 2° and 4° northeast of Ophelia (Fig. 7c).

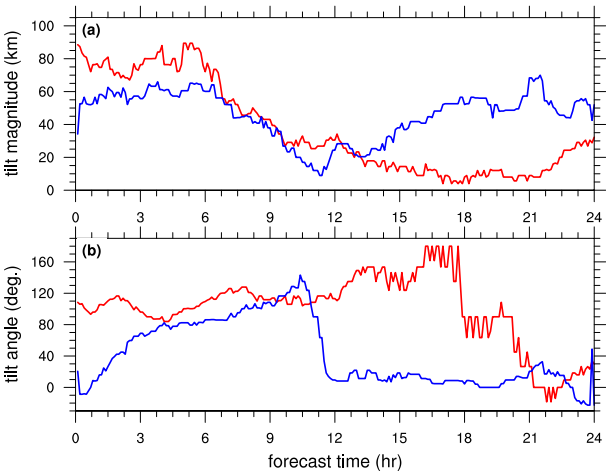

FIG. 6. Time series of (a) tilt magnitude and (b) tilt angle between the 500- and 850-hPa circulation centers of a strong member (red lines) and a weak member (blue lines).

The different initial tilt configurations have important implications for the vertical motion around Ophelia. With an initially larger tilt toward the left-of-shear quadrant, strong members have mesoscale subsidence in the upshear quadrant and mesoscale ascent in the downshear quadrant (Fig. 5a). Since the balanced response to the tilt is proportional to the magnitude of the tilt (Jones 1995), the larger tilt magnitude of strong members favors stronger vertical motions. As the vortex of the weak member is initially tilted toward the downshear quadrant, mesoscale subsidence occurs in the left-of-shear quadrant (Fig. 5b). The superposition of the mesoscale downdraft with initially drier air of weak members inhibits convective activity and moistening of the left-of-shear column. To demonstrate this, Figs. 8a,b shows time series of 6-min PW averaged within each shear-relative quadrant and within a 200-km radius (the approximate radius of largest PW differences

[5] For most parcels the initial location corresponds to their location at 0 h. However, some parcels originated outside the 4-km grid domain at 0 h. For those parcels, the original location is taken at the earliest lead time possible (i.e., 1 h for most, 6 h just for one parcel).

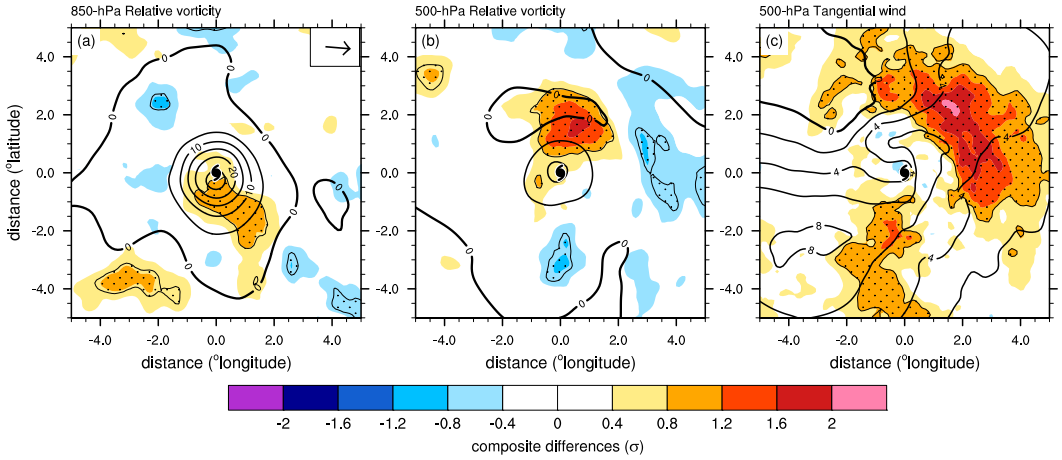

FIG. 7. Composite differences between strong and weak members (shading, every 0.4σ) for (a) 850-hPa area-averaged relative vorticity (black contours every $5 \times 10^{-5}\,s^{-1}$), (b) 500-hPa area-averaged relative vorticity (black contours every $5 \times 10^{-5}\,s^{-1}$), and (c) 500-hPa tangential wind (black contours every $2\,m\,s^{-1}$) at 0 h. Black contours represent the ensemble mean. Statistically significant results at the 95% confidence level are indicated by the stippling pattern.

in Fig. 4) of all strong and weak members. While the downshear and left-of-shear PW of strong members remain fairly constant during the first 6 h, the PW of weak members decreases 2 mm in the downshear quadrant and 4 mm in the left-of-shear quadrant. This much drier air in weak members eventually spreads to the upshear quadrant, where the PW reduces 4 mm between 6 and 12 h.

Although the initial vortex tilt direction could trigger the contrasting PW evolutions between strong and weak members, the evolution of the vortex tilt cannot solely explain the intensity changes of Ophelia. As seen in Fig. 6a, both the strong and the weak member experience a reduction in tilt magnitude during the first 12 h. The tilt magnitude of the strong member continues decreasing until reaching a minimum of 10 km at 20 h as the midlevel vortex is displaced in the opposite direction of the shear (180°, Fig. 6b). By contrast, the tilt magnitude of the weak member reaches a minimum of 18 km at 12 h (Fig. 6a), after which time the tilt magnitude increases again as the midlevel vortex returns to the downshear quadrant (0°) and is advected by the environmental shear (Fig. 6b). These tilt evolutions show that the broader, stronger, and more moist circulation of strong members allows for a faster vortex realignment than in weak members, as predicted by previous literature (Wong and Chan 2004; Riemer et al. 2013; Reasor and Montgomery 2015). However, a comparison of Fig. 6a with Fig. 2b reveals that the vertical alignment of strong members follows, but does not precede, intensification. While the increasingly large tilt magnitude of the weak member could be inhibiting intensification after 12 h, other processes must be triggering the intensification of strong members during the first 12 h.

The slow evolution of tilt differences in contrast to the rapid evolution of PW differences between strong and weak members suggests that moisture variability must be important for the intensity changes of Ophelia. A water vapor budget is used to demonstrate the processes by which moisture changes so drastically between the subsets during the first 12 h. This budget was calculated as in Part I, except the contributions to the budget were separated into shear-relative quadrants within a time period between t_0 and t_1 as follows:

$$\widetilde{\rho q_v}(t_1) - \widetilde{\rho q_v}(t_0) = -\frac{1}{A'}\int_{t_0}^{t_1}\int_{A'} \nabla_h \cdot (\rho q_v \mathbf{V}_h)\, dA'\, dt - \frac{1}{A'}\int_{t_0}^{t_1}\int_{A'} \frac{\partial(\rho q_v w)}{\partial z}\, dA'\, dt - \int_{t_0}^{t_1} (\tilde{C} - \tilde{E})\, dt + \int_{t_0}^{t_1} \tilde{B}\, dt, \qquad (2)$$

where q_v is the water vapor mixing ratio, ρ is the dry-air density, $\mathbf{V}_h$ is the horizontal wind, w is the vertical wind speed, C is the condensation, E is the evaporation, B is the contribution from the planetary boundary layer parameterization scheme, A' is the area of the quadrant, and the tilde represents an area average. In this definition of the water vapor budget, the horizontal flux convergence has contributions from both the tangential and radial flux as opposed to only the radial flux when the budget is integrated over a circular area. In the interest of evaluating the processes leading to the large water vapor differences of the left-of-shear quadrant, the budget was integrated within 200 km of Ophelia from 0 to 12 h.

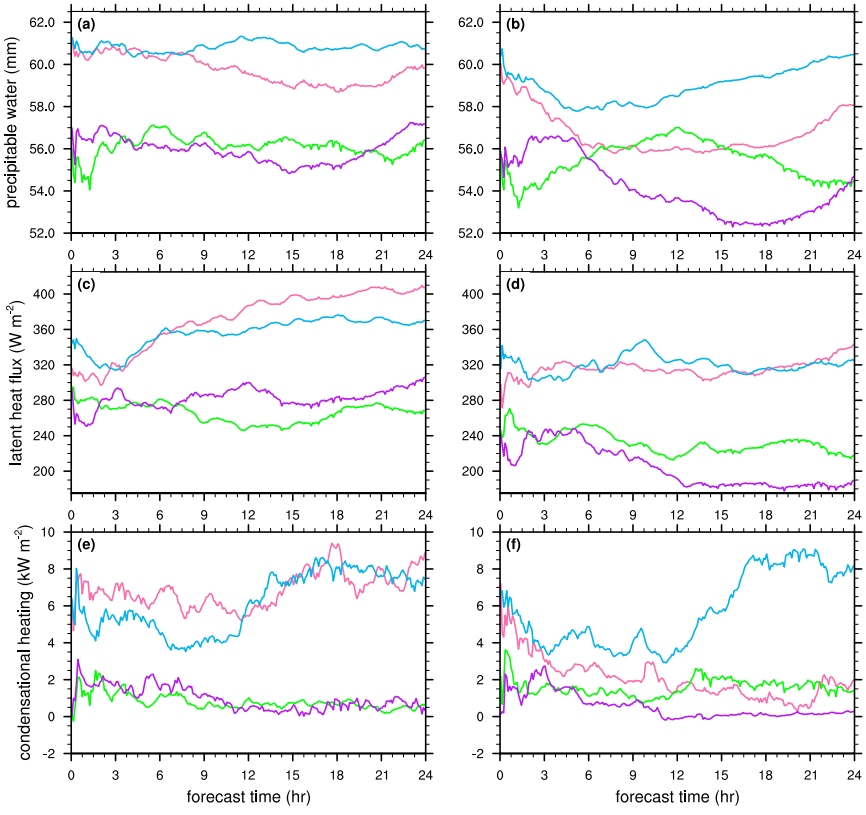

FIG. 8. Time series of (a),(b) precipitable water, (c),(d) surface latent heat flux, and (e),(f) column-integrated condensational heating averaged within each shear-relative quadrant and within 200 km from the center of Ophelia in (left) strong members and (right) weak members. Colors depict the shear-relative quadrants: left of shear (pink), downshear (light blue), right of shear (green), and upshear (purple).

Figure 9a illustrates the contrasting water vapor budgets of strong and weak members. While strong members have a net gain of left-of-shear water vapor between 1.5 and 4 km, weak members experience a net loss within the same layer. This contrast is related to noteworthy differences between the individual contributions to the water vapor budget of each subset. Strong members experience an upward redistribution of water vapor as represented by the vertical water vapor flux divergence below 4 km and vertical water vapor flux convergence above 4 km (short-dashed line of Fig. 9a). By contrast, weak members experience less redistribution of water vapor because that subset has vertical water vapor flux divergence over a deeper layer and weaker water vapor flux convergence above 6 km. The greater vertical redistribution of water vapor in strong members thus favors more sustained convection, which is evidenced by the larger condensation of strong members (long-dashed lines of Fig. 9a). Even with a greater loss of water vapor to condensation, strong members experience more left-of-shear moistening than weak members.

The horizontal flux convergence term (solid lines of Fig. 9a) also plays an important role on the contrasting evolutions of left-of-shear water vapor. As shown in Fig. 9a, strong members have stronger horizontal water vapor flux convergence from the surface up to 5.5 km. The largest separation between strong and weak members is in the lowest 2 km, where the horizontal flux convergence of weak members is nearly zero or even changes to flux divergence. To better understand this discrepancy, Fig. 9b shows a time series of the horizontal flux convergence tendency at 2-km height. Not only is the tendency of strong members twice as large as the tendency of weak members from the onset, but also the tendency of weak members reduces to zero and negative values after 4.5 h. This reduction occurs as dry air intrudes into the inner core by the storm-relative horizontal winds (Figs. 9c,d). Strong members have less dry-air intrusion, resulting in greater and more persistent water vapor flux convergence due to weaker tangential water vapor gradient through the left-of-shear quadrant.

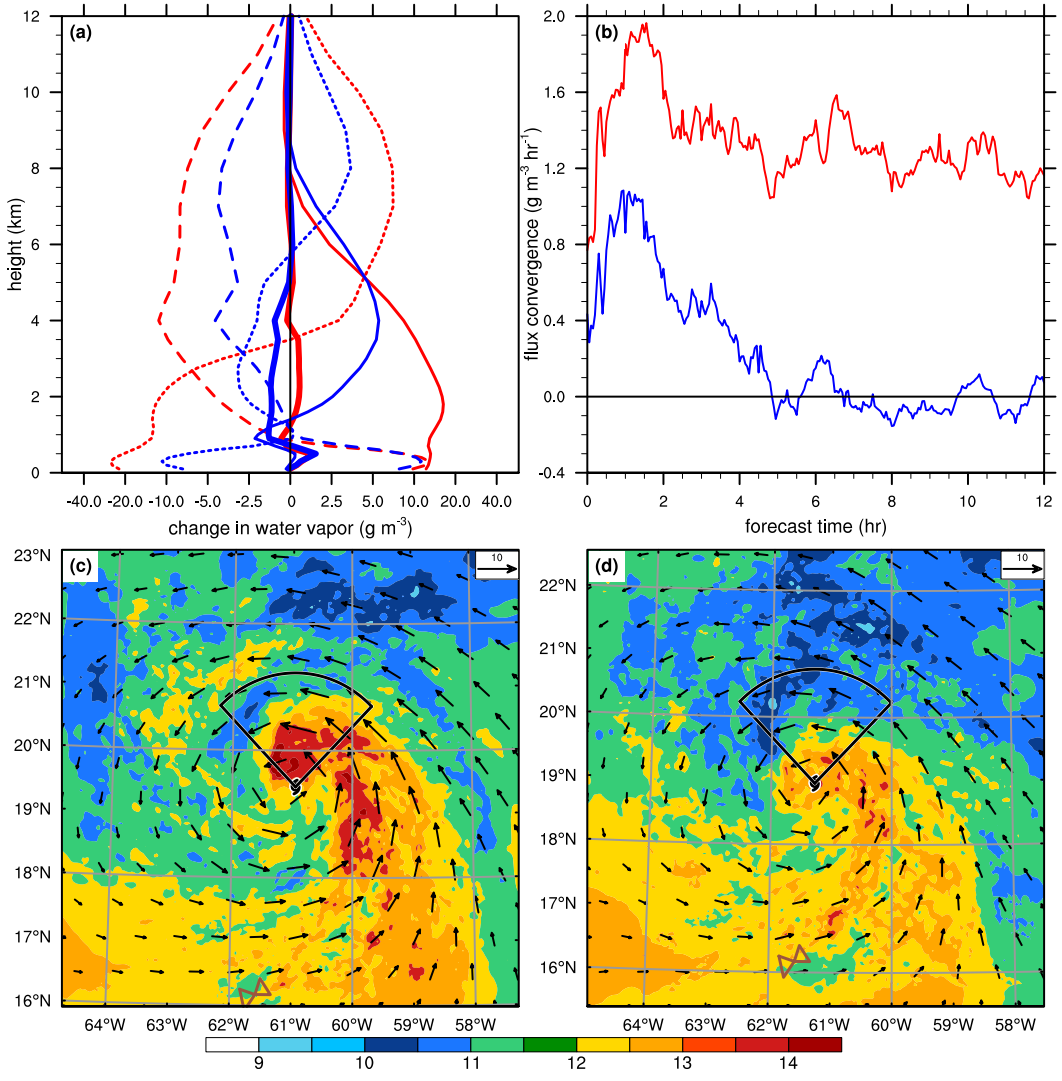

FIG. 9. (a) Vertical profiles of water vapor budget between 0 and 12 h only within the left-of-shear quadrant of strong (red lines) and weak (blue lines) members. Thick solid lines represent the sum of all contributions, while thin lines represent horizontal flux convergence (solid lines), vertical flux convergence (short-dashed lines), and the sum of condensation, evaporation, and planetary boundary layer tendency (long-dashed lines). (b) Time series of the 2-km area-averaged horizontal water vapor flux convergence within a 200-km radius of strong (red line) and weak (blue line) members. (c),(d) Storm-centered 6-h forecast of 2-km water vapor density (shading, every 0.5 g m^{-3}) and water vapor flux (arrows, scaled by 1.0×10^5 g m^{-2} h^{-1}). Shown in (c) is the composite of strong members and in (d) is the composite of weak members. The black lines depict the limits of the left-of-shear quadrant within a 200-km radius of Ophelia.

As a consequence of less subsiding air, less dry-air intrusion, and more moisture gain in the left-of-shear quadrant, strong members can promote more convection and help align the vortex. Rappin and Nolan (2012) demonstrated that when the vertical shear direction is counteraligned with the surface mean flow (as in this case; Fig. 1), enhanced surface latent heat fluxes to the left of the shear moisten the midtroposphere through shallow convection, allow sustained convection to propagate cyclonically around the TC, and accelerate the alignment of the tilted vortex. In the present case, the strongest latent heat fluxes occur both downshear and left of the shear vector of strong and weak members (Figs. 8c,d). However, the latent heat fluxes of strong members increase over time (except right of shear) while the latent heat fluxes of weak members remain nearly constant or even decrease over time. The enhanced surface fluxes of strong members, along with greater midtropospheric moisture, likely strengthen the shear-induced ascending motions in the downshear and

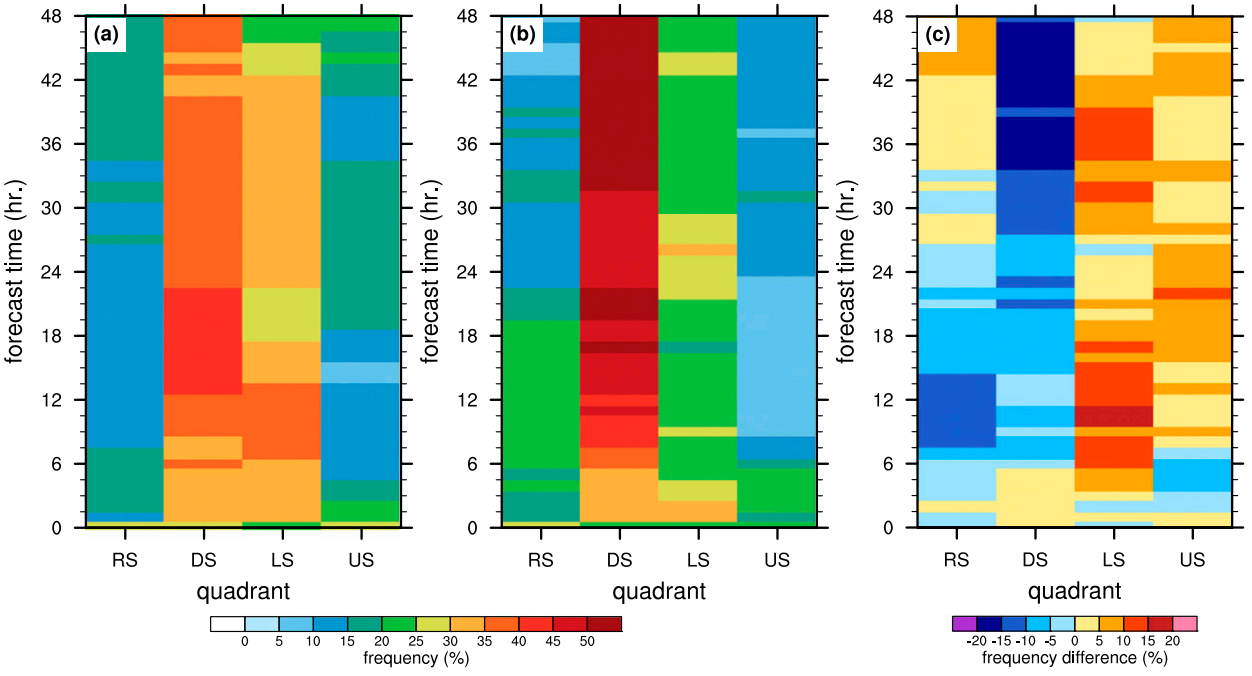

FIG. 10. Time–quadrant analysis of the hourly distributions of convective updrafts between 500 and 850 hPa. The distributions are decomposed into shear-relative quadrants, namely, right of shear (RS), downshear (DS), left of shear (LS), and upshear (US). The distributions of (a) strong and (b) weak members normalized by the total amount of points used at every hour (shading, every 5%). (c) The difference between the strong and weak members' distributions (shading, every 5%).

left-of-shear quadrants (Fig. 8e). These favorable conditions could also support the azimuthal propagation of convection around the TC, which helps realign the vortex as suggested by Rappin and Nolan (2012). Weak members see an overall reduction of convection up to 12 h, after which time convection mostly occurs in the downshear quadrant (Fig. 8f).

To further compare the preferred location of convection in strong and weak members, hourly distributions of convective updrafts are considered in a shear-relative framework. These distributions separate the convective updrafts (defined as positive 500–850-hPa vertical velocity and cloud mixing ratio greater than $1 \times 10^{-5}\,\mathrm{g\,kg^{-1}}$) into 90° azimuthal bins around Ophelia. Convective updrafts are counted only within a 200-km radius of Ophelia for consistency with the previous diagnoses. Similar to the vertically integrated condensational heating, convective updrafts are more abundant in the downshear and left-of-shear quadrants of strong members (Fig. 10a) but primarily in the downshear quadrant of weak members (Fig. 10b). This difference becomes clear between 6 and 33 h when strong members have up to 20% more left-of-shear updrafts and up to 15% less downshear updrafts than weak members (Fig. 10c). Additionally, strong members have more updrafts in the left-of-shear quadrant and less updrafts in the right-of-shear quadrant (Fig. 10c).

Despite the preference for downshear convection of weak members, those members do not experience a downshear reformation and intensification as noted by previous studies (Molinari et al. 2006; Molinari and Vollaro 2010). Instead, weak members lack a mechanism to moisten the midtroposphere and promote convection in the left-of-shear and upshear quadrants, thus becoming more tilted and asymmetric over time. This subset behaves similarly to Tropical Storm Edouard (2002), which was unable to intensify following a period of downshear convective downdrafts because of the presence of dry air in the upshear quadrant (Molinari et al. 2013). On the contrary, the higher occurrence of left-of-shear updrafts in strong members seems to provide more favorability for intensification. This result is more consistent with the study of Chen and Gopalakrishnan (2015) which showed that the rapid intensification of Hurricane Earl was triggered by convective bursts to the left of the shear vector. The next section will further investigate the role of left-of-shear convection in the intensification of Ophelia.

5. Role of left-of-shear convection

A potential explanation for the different intensity changes of Ophelia can be linked to the interaction between convective processes and the nearby upper-tropospheric

trough. Recall from Fig. 3d that strong members have a more favorable interaction with the upper-tropospheric trough after 12 h. The previous section demonstrated that strong members have more moisture and more convection to the left of the shear vector even prior to the significant differences in EFC. Given that the upper-tropospheric trough is initially located upstream of Ophelia (to be shown below), the greater left-of-shear convection could alter the upper-tropospheric trough in such way that strong members import more cyclonic momentum from the trough into the TC. This possibility is explored here with storm-centered composites of 250-hPa divergence and 250-hPa PV.[6]

Upper-tropospheric differences between strong and weak members highlight the rapid and distinct evolution of the upper-tropospheric flow (Fig. 11). Initially, strong and weak members have similar upper-tropospheric divergence and PV, except strong members have a slightly weaker trough to the northwest of Ophelia (Figs. 11a,b). Significant differences appear at 6 h when strong members have 0.8–1.6σ stronger upper-level divergence north (left of shear) of Ophelia (Fig. 11c). This region of stronger divergence is located cyclonically downwind of the region of stronger near-surface convergence (not shown) and is consistent with the greater left-of-shear and downshear convection. Also by 6 h, strong members have 1.6σ greater PV west (upshear) of Ophelia and 1.2σ less PV approximately 2°–8° north of Ophelia (Fig. 11d). These composite differences increase in magnitude and coverage, such that by 12 h strong members have 1.6σ stronger upper-level divergence concentrated to the north of Ophelia (Fig. 11e). Strong members also have up to 1.2σ less PV to the north of Ophelia as well as up to 2.0σ greater PV to the west and right above the TC center (Fig. 11f).

Based on the upper-tropospheric composites, one can conclude that the enhanced moisture and convection of strong members enhances the anticyclonic outflow and prevents disruption from the trough. With more negative PV and stronger divergence directly above the left-of-shear convection, negative PV advection by the divergent winds can tighten the PV gradient and keep the upper-tropospheric trough away from the TC. In fact, the composite 250-hPa PV and storm-relative winds at 24 h reveal that the trough of strong members is forced to wrap cyclonically around Ophelia (Fig. 12a), thus resembling the favorable TC–trough interaction documented in Hanley et al. (2001). By contrast, the trough of weak members remains undisturbed and is associated with stronger storm-relative zonal flow west of Ophelia (Fig. 12b). These different configurations explain the different EFC noted in Fig. 3d, because strong members have stronger anticyclonic outflow north of Ophelia and stronger cyclonic inflow west of Ophelia (Figs. 12a,b). In other words, strong members export more anticyclonic momentum away from the TC vortex and import more cyclonic momentum from the trough into the TC vortex.

The more favorable TC–trough interaction of strong members allows this subset to continue its trend of intensification, while the less favorable TC–trough interaction of weak members is another factor to inhibit the intensification of this subset. By forcing the trough away from the vortex, strong members have a weaker trough-induced shear (Fig. 3a) that supports a more vertically aligned vortex (Fig. 6a) and less potential for dry-air intrusion (Figs. 9c,d). For example, the midtropospheric storm-relative winds of strong members depict a closed circulation right above the lower-tropospheric center of circulation at 24 h (Fig. 12c). In contrast, the midtropospheric storm-relative winds of weak members depict a closed circulation displaced to the east (downshear) of the lower-tropospheric center of circulation (Fig. 12d). Consequently, weak members have stronger storm-relative flow across the TC center (Figs. 12c,d) that potentially advects dry air and limits convection above the lower-tropospheric center (e.g., Tang and Emanuel 2012; Davis and Ahijevych 2012). The stronger downshear convection in this subset potentially contributes to a vortex tilt reduction, but the location of convection is not optimal for reducing the effects of the upper-tropospheric trough.

6. Vorticity budget

Besides affecting the interaction between Ophelia and the upper-tropospheric trough, the distribution of convection around the TC can also affect the inner-core circulation of Ophelia. Part I demonstrated that the strengthening and deepening of the inner-core vortex of Katia resulted from a combination of deep vortex stretching and tilting of horizontal vorticity. These two processes were linked to the amount of convection around Katia, where strong members had more convection and thus stronger stretching and tilting. To link the distribution of convection to the inner-core vortex of Ophelia, a vorticity budget was calculated as in Part I. In this case, the domain was reduced to 150 km × 150 km

[6] Model output was only available up to 200 hPa, but PV was computed at 250 hPa to maximize the number of isobaric levels used in the calculation. Also, the PV and divergence fields were averaged within 1° (approximately 100 km) of each grid point in order to remove the noise associated with high-resolution finite derivatives.

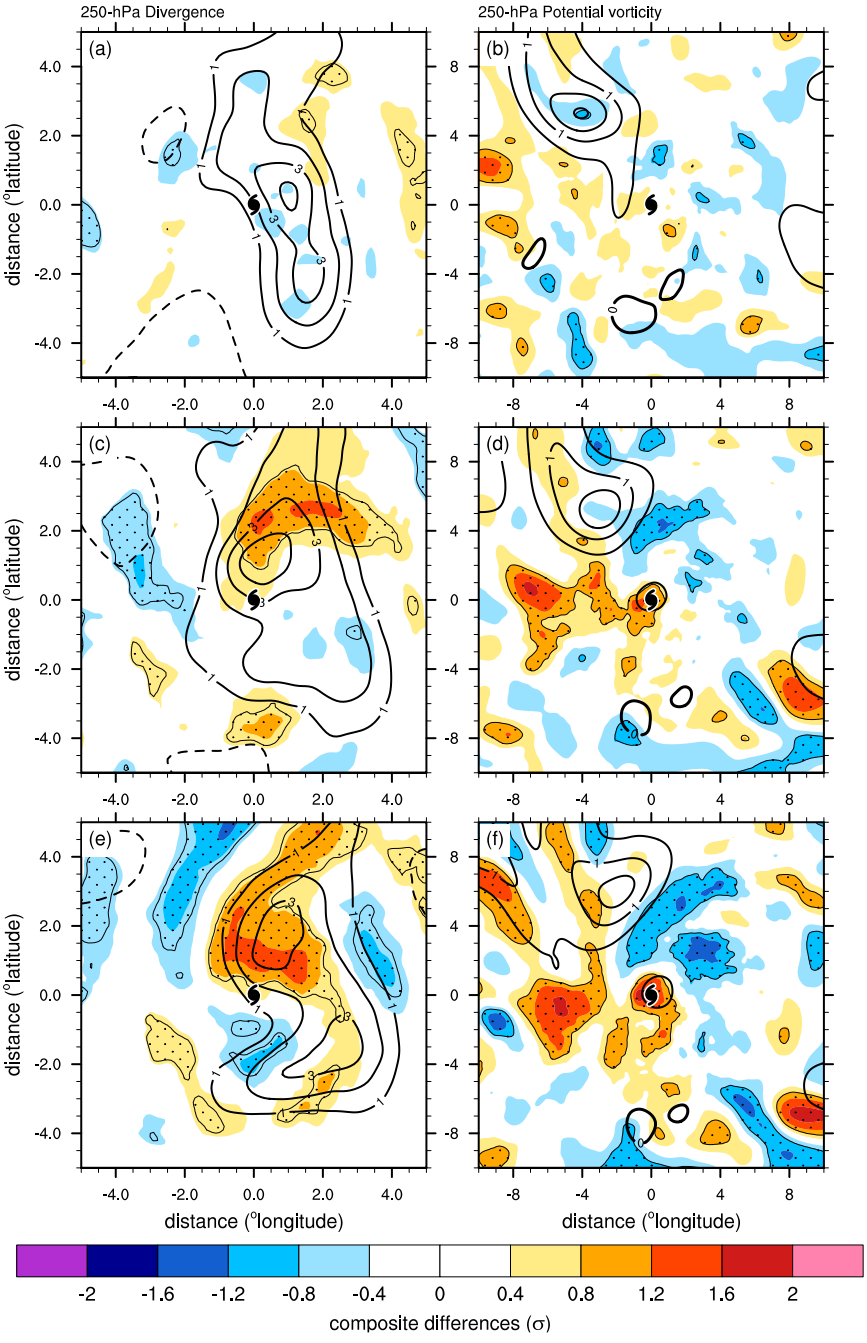

FIG. 11. Composite differences between strong and weak members (shading; every 0.4σ) for (a),(c),(e) 250-hPa divergence (black contours every 1.0 $\times$ 10^{-5} s^{-1}) and (b),(d),(f) 250-hPa potential vorticity [black contours every 0.5 PVU (1 PVU = 1.0 $\times$ 10^{-6} m^2 s^{-1} K kg^{-1})] at (a),(b) 0, (c),(d) 6, and (e),(f) 12 h. Black contours represent the ensemble mean. Statistically significant results at the 95% confidence level are indicated by the stippling pattern.

about the 850-hPa center of Ophelia because the radius of maximum winds of Ophelia was approximately 75 km at 0 h. Two different periods were considered: from 0 to 12 h to study the initial intensity changes and from 12 to 24 h to study the intensification of strong members after this subset had greater left-of-shear convection, smaller tilt, and stronger EFC.

During the 0–12-h period, the area-averaged vorticity of both strong and weak members strengthens at all levels considered, but strong members have a

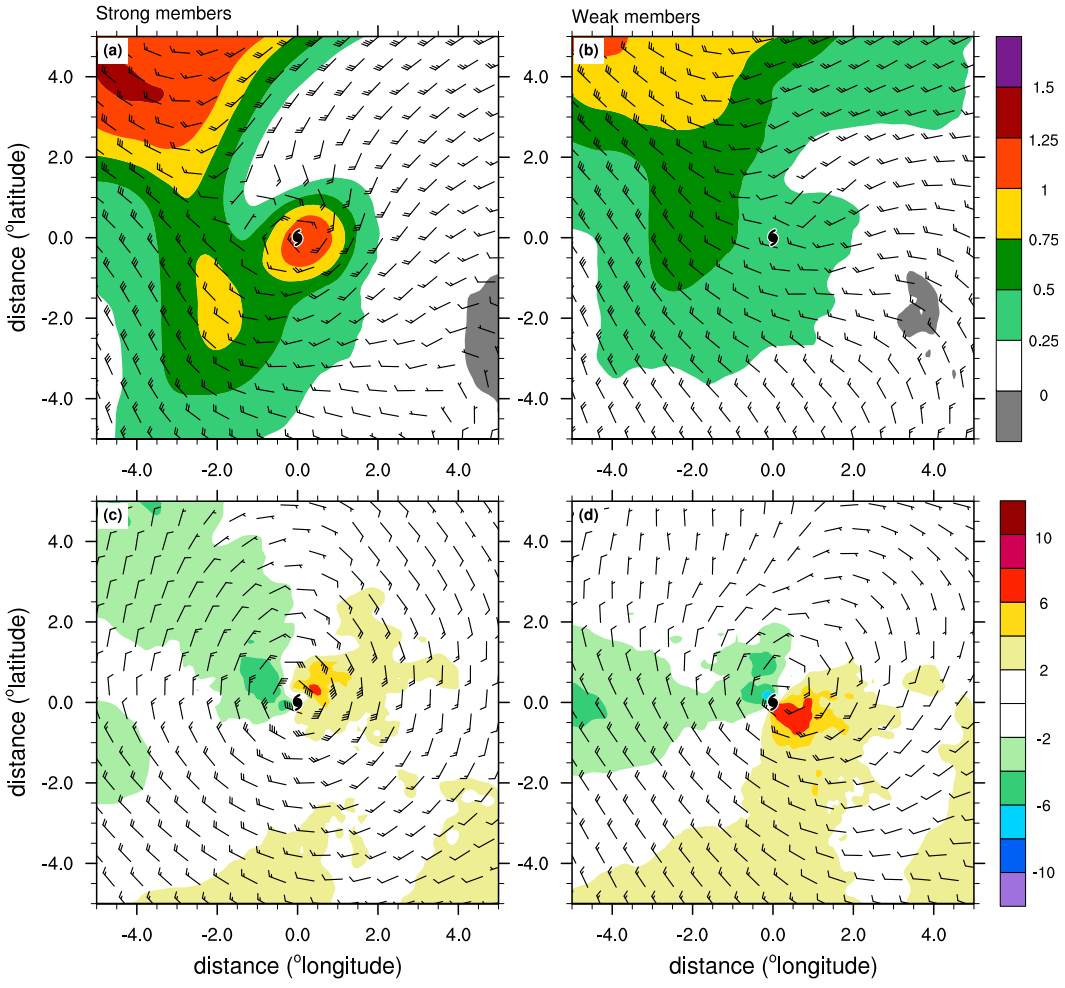

FIG. 12. (a),(b) Latitude–longitude analysis of composite 250-hPa potential vorticity (shading, every 0.25 PVU) and storm-relative winds (barbs, long wind barbs represent 10 m s^{-1}). (c),(d) As in (a),(b), but for 500-hPa storm-relative radial wind (shading, every 2 m s^{-1}) and storm-relative winds (barbs, long wind barbs represent 10 m s^{-1}) at 24 h. (left) The composites of strong members and (right) the composites of weak members.

greater change in area-averaged vorticity than weak members (Fig. 13a). The summation of the individual tendencies yields a change in area-averaged vorticity that is similar in shape and magnitude, albeit larger, than the area-averaged vorticity change between 0 and 12 h. Investigating the individual contributions shows that strong members have stronger vortex stretching in the lower troposphere (from 900 to 850 hPa) and stronger tilting of horizontal vorticity in the midtroposphere (from 875 to 400 hPa; Fig. 13b). The eddy vorticity flux is small and negative at most levels considered, but with similar magnitude in both subsets. This analysis demonstrates that the strengthening of the lower-tropospheric circulation is primarily driven by vortex stretching, which is consistent with the low-level convergence associated with stronger vertical motion in strong members.

An intriguing aspect of the budget is that the strengthening of the area-averaged vorticity above 800 hPa is dominated by tilting of the horizontal vorticity. This greater tilting is associated with a positive correlation between the vertical motion and the component of horizontal vorticity normal to the domain, especially left of shear and downshear of Ophelia. For example, the 12-h forecast at 500 hPa shows that strong members have upward motion collocated with horizontal vorticity pointing outward from Ophelia (Fig. 14a). As discussed by Davis and Galarneau (2009), updrafts at the boundary of the vorticity box would tilt the outward pointing horizontal vorticity and generate cyclonic relative vorticity inside the box. This generation of cyclonic relative vorticity within a 75-km radius potentially helps the alignment of the vortex as the tilt magnitude decreases during this period (Fig. 6a). Weak members, however, generate less relative vorticity

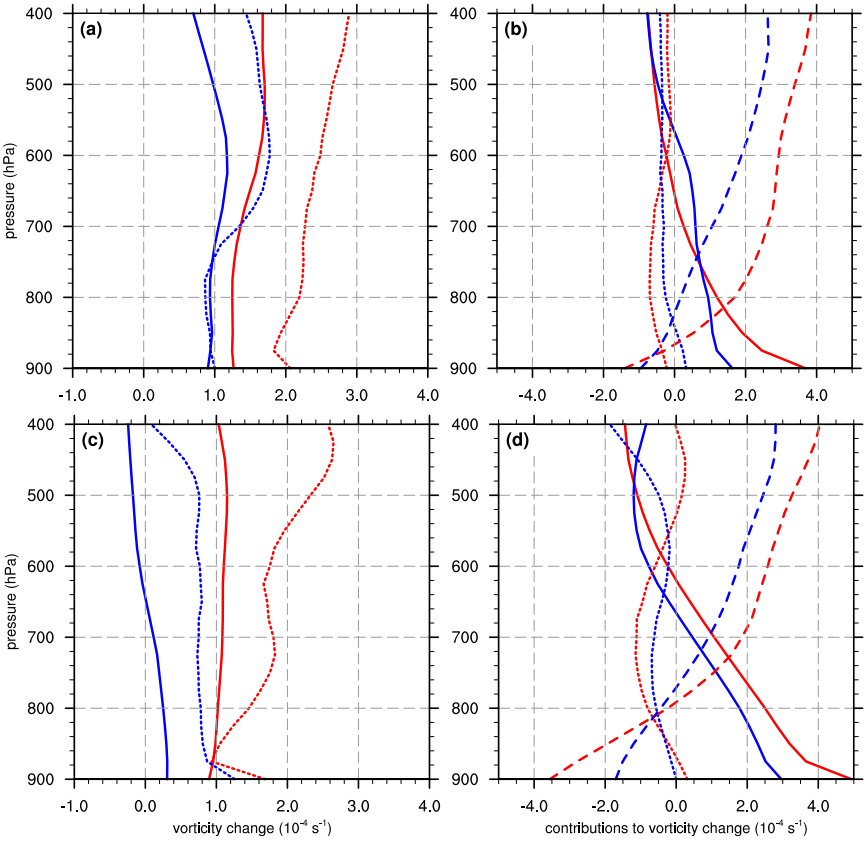

FIG. 13. Vertical profiles of vorticity budgets during (a),(b) 0–12 and (c),(d) 12–24 h. (left) The area-average vorticity change (solid lines) and the sum of all contributions to the vorticity equation (dashed lines). (right) The individual contributions to the vorticity budget: stretching and friction (solid lines), eddy vorticity flux (short-dashed lines), and tilting (long-dashed lines). In all panels red (blue) lines represent the composite of strong (weak) members.

through tilting owing to both weaker upward motion and stronger downward motion collocated with outward-pointing horizontal vorticity (Fig. 14b). This result further supports the crucial role of the distribution of convection during the intensity changes of Ophelia within the AHW ensemble.

During the 12–24-h period, the area-averaged vorticity of strong members strengthens at all levels considered, while the area-averaged vorticity of weak members weakens above 600 hPa (Fig. 13c). The summation of the individual tendencies once again captures the general shape of the profile of the vorticity change within the box. Evaluating the individual terms shows a similar pattern as during the 0–12-h period, except now strong members have more positive stretching than weak members below 600 hPa and more negative vortex stretching above 500 hPa (Fig. 13d). This profile represents deeper mass flux and convection in strong members, which is consistent with the greater upper-level divergence discussed earlier. The tilting term once again dominates the cyclonic vorticity generation in the mid- and upper troposphere. Negative eddy vorticity flux partially offsets the cyclonic vorticity generation by stretching and tilting, but the stretching and tilting terms of strong members are much larger than the eddy term resulting in a net positive vorticity change.

7. Sensitivity experiments

Based on the diagnoses of strong and weak members, variability of convection and large-scale features (e.g., trough) in the initial conditions (ICs) can lead to different intensity changes of sheared TCs. This hypothesis is tested by creating an ensemble of perturbed ICs and integrating the model forward 72 h, as in Part I. The IC metrics in this case are the 10-m convergence east of Ophelia and 250-hPa PV northwest of Ophelia. The 10-m convergence was chosen to represent variability in convection that initiates downshear and deepens left of the shear vector. This IC metric consisted of an average of the 10-m convergence only within grid points where the difference between strong and weak members was statistically significant (not shown). Three

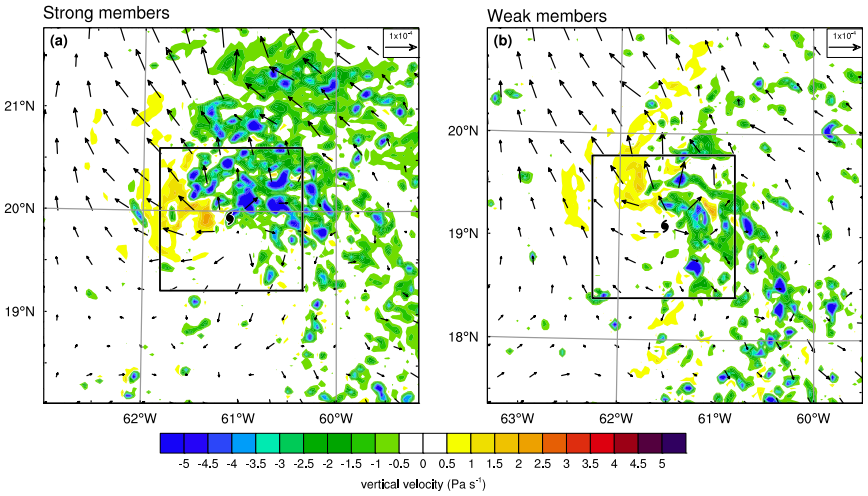

FIG. 14. Storm-centered 12-h forecast of 500-hPa vertical velocity (shading, every 0.5 Pa s^{-1}) and 500-hPa horizontal vorticity (vectors, scaled by 1.0×10^{-4} s^{-1}) for the (a) strong members and (b) weak members. The black box depicts the 150 km × 150 km box used to calculate the vorticity budget.

experiments were performed for this IC metric to test the impact of perturbing all state variables (named ALL), only water mixing ratios (named MOIST), or only dynamic variables (named DRY) in response to a hypothetical observation of 10-m convergence. An additional experiment perturbed all state variables according to a change in the 250-hPa PV to investigate the influence of variability in the upper-tropospheric trough. This IC metric was defined as the average of all grid points where the PV exceeded 0.5 PVU northwest of Ophelia (cf. Fig. 11b). All experiments will be analyzed with respect to the 96-member ensemble mean because the sensitivity experiments apply to all members within the ensemble.

The first experiment perturbs all state variables according to a hypothetical observation of stronger 10-m convergence, akin to stronger convection, than in the control simulation. For this experiment, the amplitude of the IC perturbation [i.e., α in Eq. (6) of Part I] is $0.5\sigma_{IC}$, where σ_{IC} is the standard deviation of the IC metric. The ICs respond to the hypothetical observation as expected because the initial ensemble-mean 10-m convergence strengthens by up to 0.9×10^{-5} s^{-1} to the east and north of Ophelia (Fig. 15a). This experiment has the desired effect of increasing the left-of-shear convection as shown by the greater 0–6-h accumulated precipitation north of Ophelia (Fig. 15b). Because all state variables are perturbed to respond to the IC metric, the initial 850-hPa circulation within 2° of the Ophelia is also stronger in the sensitivity experiment than in the control simulation (Fig. 15c). With stronger lower-tropospheric convergence and circulation in the ICs, the 850-hPa circulation at 72 h strengthens by more than 1.5×10^{-5} s^{-1} in the sensitivity experiment (Fig. 15d).

Repeating the same experiment, but changing the amplitude of the perturbation between $-1.5\sigma_{IC}$ and $1.5\sigma_{IC}$, confirms the sensitivity of the intensity forecasts of Ophelia to the initial strength of the downshear convection. Results from the ALL experiments are summarized in Fig. 16 through a comparison of the 72-h ensemble-mean MSLP forecast changes predicted by the ensemble-based sensitivity analysis [Eq. (6) from Part I; predicted change] and given by the difference between the sensitivity experiment and the control simulation (actual change). Generally, there is good agreement between the actual and predicted 72-h MSLP changes. Since the predicted MSLP change is proportional to the amplitude of the IC metric, Fig. 16 demonstrates that perturbing the ICs in response to stronger (weaker) 10-m convergence results in a stronger (weaker) TC with 0–4-hPa lower (higher) MSLP by 72 h. The ensemble spread of the control 72-h forecast is 8.4 hPa; thus, a $1\sigma_{IC}$ change in the initial 10-m convergence accounts for 36% of the ensemble MSLP standard deviation. Comparing the ALL, MOIST, and DRY experiments reveals that the greatest MSLP changes stem from perturbations to all state variables and the smallest MSLP changes result from perturbations only to water mixing ratios. These results suggest that the initial dry dynamical differences (i.e., shear-forced ascent) dominate the variability in amount and strength of convection around Ophelia; however, the initial moist differences play a

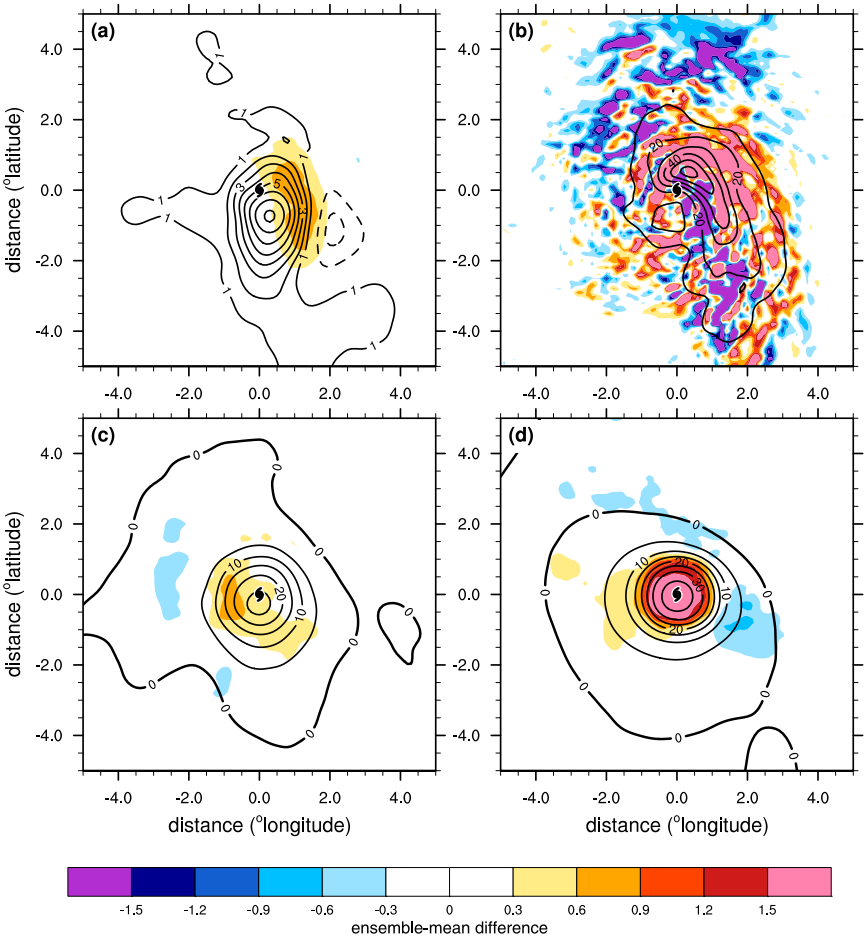

FIG. 15. Latitude–longitude analysis of ensemble-mean differences between the sensitivity experiment and the control simulation (shading) and the ensemble mean from the control simulation (contours). (a) The 0-h 10-m convergence (shading every $0.3 \times 10^{-5}\,s^{-1}$ and contours every $1.0 \times 10^{-5}\,s^{-1}$). (b) The 0–6-h precipitation (shading every 0.3 mm and contours every 10 mm). The 850-hPa area-averaged vorticity (shading every $0.3 \times 10^{-5}\,s^{-1}$ and contours every $5 \times 10^{-5}\,s^{-1}$) at (c) 0 and (d) 72 h.

secondary role in deepening the convection to the left of the shear vector.

The second experiment perturbs the ICs according to a hypothetical observation of the 250-hPa PV around the upper-tropospheric trough. Figure 16 shows that both the predicted and actual MSLP changes are substantially smaller than the previous experiment even though the perturbation amplitudes also range between $-1.5\sigma_{IC}$ and $1.5\sigma_{IC}$. Perturbing the ICs to respond to either a stronger or weaker upper-tropospheric trough results in less than 0.5-hPa change in the 72-h MSLP, which is only 6% of the ensemble spread. This result is somewhat contradictory to the findings of Hanley et al. (2001), which showed that the strength of an upper-tropospheric trough could determine whether or not a TC would intensify following a TC–trough interaction. Based on the results of the sensitivity experiments, one can conclude that the outcome of the TC–trough interaction in this case depends more on the interaction between small-scale convective processes and the large-scale flow than solely on the strength of the upper-tropospheric trough.

8. Summary and conclusions

This study employed 96 high-resolution, full physics, ensemble forecasts to investigate intensity changes of weak tropical storms in environments characterized by moderate vertical wind shear. The ensemble forecasts were produced with the Advanced Hurricane WRF (AHW) Model and initialized from a 6-hourly cycling data assimilation system. Two weak tropical storms were simulated with the 96-member AHW ensemble: Katia

(2011), which encountered easterly 200–850-hPa shear, and Ophelia (2011), which encountered 200–850-hPa westerly shear. Five-day intensity forecasts for both storms were characterized by large uncertainty, with ensemble members predicting the TCs would either intensify, weaken, or even dissipate. Physical processes behind the large uncertainty in intensity forecasts were investigated by comparing two subsets of 12 members that predicted either intensification or weakening (strong and weak members hereafter). This method was applied in Part I to study the intensity changes of Katia, while this second part focused on the intensity changes of Ophelia.

A comparison of strong and weak members revealed small variability in large-scale conditions but substantial variability in the asymmetric structure of Ophelia. Using diagnoses of area-averaged quantities within a 500-km radius of Ophelia, it was found that strong members had greater PW only from 0 to 6 h, weaker 200–850-hPa shear magnitude after 24 h, and cooler SSTs throughout the forecast. The location and timing of environmental PW differences were further investigated to compare the relationship between water vapor and convection initiation of strong and weak members. A storm-centered analysis showed that strong members were initialized with greater midtropospheric water vapor within 2° of the downshear quadrant. Moisture differences rotated with time, such that strong members had greater midtropospheric water vapor in the left-of-shear quadrant by 12 h and in the upshear quadrant by 24 h. The lack of significant PW differences in the environmental diagnoses after 6 h was thus related to the asymmetric location of water vapor around strong and weak members.

The contrasting evolution of moisture around Ophelia was linked to the initial tilt of the vortex because strong members were initially tilted toward the north (left of shear), while weak members were initially tilted toward the east (downshear). These different tilt configurations were associated with mesoscale subsidence in the upshear quadrant and mesoscale ascent in the downshear quadrant of strong members but mesoscale subsidence in the left-of-shear quadrant of weak members. Consequently, weak members experienced a substantial drying of the left-of-shear and downshear quadrants due to the absence of a lifting mechanism to moisten the midtroposphere. On the contrary, convection of strong members was favored around Ophelia via enhanced midtropospheric moisture and surface latent heat fluxes similarly to the case of counteraligned shear and surface winds of Rappin and Nolan (2012). This propagation was not evident in the case of weak members even though the shear and the surface winds were also counteraligned, but Rappin and Nolan (2012) were concerned with TC genesis in an idealized framework. A more complicated analysis combining the sensitivities of shear direction, tilt direction, and dry-air location for a weak tropical storm could clarify these discrepancies.

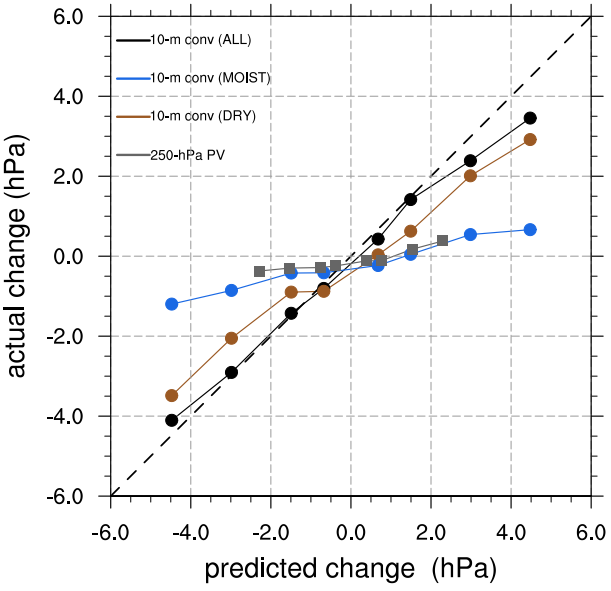

FIG. 16. Comparison between the predicted and actual ensemble-mean 72-h MSLP changes within the 96-member AHW ensemble (see text for details). Each symbol represents an individual experiment with a prescribed perturbation amplitude to the initial-condition metric. Black, blue, and brown circles represent the ALL, MOIST, and DRY experiments, respectively, corresponding to perturbations to the initial 10-m convergence. Gray squares represent the experiments corresponding to perturbations to the initial 250-hPa PV. The dashed black line depicts a 1:1 relationship between the predicted and actual MSLP forecast changes.

Despite the enhanced distribution of convection around Ophelia, strong members remained highly asymmetric during their intensification. Most convective updrafts within a 200-km radius of Ophelia occurred in the left-of-shear and downshear quadrants of strong members. The location of convection was crucial for the interaction between Ophelia and a nearby upper-tropospheric trough. With more and stronger convection in the left-of-shear quadrant, strong members also had greater upper-level divergence and more negative PV that strengthened the upper-tropospheric anticyclonic outflow and forced the trough to wrap around Ophelia. This interaction resulted in 5–10 $m\,s^{-1}\,day^{-1}$ significantly stronger eddy momentum flux convergence in strong members as that subset was exporting more anticyclonic momentum away from the TC, while importing more cyclonic momentum from the trough into the TC.

Furthermore, a vorticity budget revealed that the amount and location of convection of strong members contributed to stronger vortex stretching and tilting of horizontal vorticity that strengthened and deepened the

circulation of Ophelia. The greater tilting of the horizontal vorticity was a result of the correlation between upward motion and the horizontal vorticity due to the upper-tropospheric trough. From this perspective, the outcome of a TC–trough interaction depends not only on the size and strength of the PV associated with the trough, as stated by Hanley et al. (2001), but also on the interaction between convection and the trough-induced shear as suggested by Shu et al. (2014). This conclusion was also supported by sensitivity experiments in which AHW forecasts with perturbed initial conditions had greater MSLP changes in response to variability of the downshear convection than in response to variability of the upper-tropospheric trough.

Katia and Ophelia had similar MSLP and deep-layer shear magnitudes when the forecasts were initialized; however, diagnoses of their intensity changes share both similarities and differences. Both cases demonstrated that variability in the initial moisture can promote variability in the intensity forecasts of sheared TCs. However, the horizontal and vertical location of the moisture variability differed between the cases. For Katia, enhanced lower-tropospheric water vapor to the right of the shear vector promoted buoyant updrafts that moistened the middle troposphere. For Ophelia, enhanced midtropospheric moisture in the downshear and left-of-shear quadrants supported the shear-forced convection. Despite the differences in the initial location of moisture variability, ultimately both cases were characterized by deep convective updrafts that aided intensification via deep vortex stretching and tilting of horizontal vorticity. The timing and rate of intensification, however, were also different between the cases. Strong members of Katia only deepened less than 10 hPa between 0 and 48 h, while strong members of Ophelia deepened approximately 25 hPa during the same period. One potential explanation is that intensification in moderately sheared environments occurs more rapidly once the midtroposphere, particularly to the left of the shear vector, is moistened enough to support sustained convection. Another possible explanation relies on the profile of environmental winds; while Katia experienced substantial shear in the lower troposphere (between 850 and 600 hPa), Ophelia experienced substantial shear in the upper troposphere (between 600 and 200 hPa). Recent work by Wang et al. (2015) suggests that shear in the lower troposphere can be more disruptive for TC intensity than shear in the upper troposphere.

Overall, this work suggests that observations from the three-dimensional moisture and wind fields could prove useful for better understanding and predicting TC intensification in sheared environments. Relatively large water vapor uncertainty in the initial conditions, combined with different TC kinematic structures of Katia and Ophelia, was instrumental in causing large intensity uncertainty within these forecasts. It is important to recognize that the initial condition uncertainty of the AHW ensemble was the result of a cycling ensemble data assimilation system with limited in situ observations (satellite radiance was not assimilated). Consequently, the AHW analysis errors were likely larger than operational analysis errors owing to the growth of forecast errors from previous cycles. Moreover, it is also possible that cases like Katia and Ophelia are inherently difficult to predict because of the processes involved in TC intensification despite moderate shear. Future work will further explore the joint role of water vapor and vortex structure during intensity changes of sheared TCs by isolating those factors in an idealized modeling framework.

Acknowledgments. The authors thank Thomas Galarneau for providing code to remove the TC vortex and calculate environmental shear. Comments from the reviewers of both parts substantially improved the quality of this study. The authors also acknowledge the NOAA Research and Development High Performance Computing Program (http://rdhpcs.noaa.gov) for providing computing and storage resources that have contributed to the research results reported within this paper. This research was funded by the National Science Foundation Graduate Research Fellowship Grant DGE 1060277, NOAA Awards NA12NWS4680003 and NA14OAR4830172, and the Significant Opportunities in Atmospheric Research and Science (SOARS) program.

REFERENCES

Avila, L. A., and S. R. Stewart, 2013: Atlantic hurricane season of 2011. *Mon. Wea. Rev.*, **141**, 2577–2596, doi:10.1175/MWR-D-12-00230.1.

Cavallo, S. M., R. D. Torn, C. Snyder, C. Davis, W. Wang, and J. Done, 2013: Evaluation of the Advanced Hurricane WRF data assimilation system for the 2009 Atlantic hurricane season. *Mon. Wea. Rev.*, **141**, 523–541, doi:10.1175/MWR-D-12-00139.1.

Chen, H., and S. G. Gopalakrishnan, 2015: A study on the asymmetric rapid intensification of Hurricane Earl (2010) using the HWRF system. *J. Atmos. Sci.*, **72**, 531–550, doi:10.1175/JAS-D-14-0097.1.

Davis, C., and L. F. Bosart, 2002: Numerical simulations of the genesis of Hurricane Diana (1984). Part II: Sensitivity of track and intensity prediction. *Mon. Wea. Rev.*, **130**, 1100–1124, doi:10.1175/1520-0493(2002)130<1100:NSOTGO>2.0.CO;2.

——, and T. J. Galarneau, 2009: The vertical structure of mesoscale convective vortices. *J. Atmos. Sci.*, **66**, 686–704, doi:10.1175/2008JAS2819.1.

——, and D. A. Ahijevych, 2012: Mesoscale structural evolution of three tropical weather systems observed during PREDICT. *J. Atmos. Sci.*, **69**, 1284–1305, doi:10.1175/JAS-D-11-0225.1.

——, and Coauthors, 2008a: Prediction of landfalling hurricanes with the Advanced Hurricane WRF model. *Mon. Wea. Rev.*, **136**, 1990–2005, doi:10.1175/2007MWR2085.1.

——, S. C. Jones, and M. Riemer, 2008b: Hurricane vortex dynamics during Atlantic extratropical transition. *J. Atmos. Sci.*, **65**, 714–736, doi:10.1175/2007JAS2488.1.

——, W. Wang, J. Dudhia, and R. Torn, 2010: Does increased horizontal resolution improve hurricane wind forecasts? *Wea. Forecasting*, **25**, 1826–1841, doi:10.1175/2010WAF2222423.1.

DeHart, J. C., R. A. Houze, and R. F. Rogers, 2014: Quadrant distribution of tropical cyclone inner-core kinematics in relation to environmental shear. *J. Atmos. Sci.*, **71**, 2713–2732, doi:10.1175/JAS-D-13-0298.1.

DeMaria, M., 1996: The effect of vertical shear on tropical cyclone intensity change. *J. Atmos. Sci.*, **53**, 2076–2088, doi:10.1175/1520-0469(1996)053<2076:TEOVSO>2.0.CO;2.

Dolling, K. P., and G. M. Barnes, 2012: The creation of a high equivalent potential temperature reservoir in Tropical Storm Humberto (2001) and its possible role in storm deepening. *Mon. Wea. Rev.*, **140**, 492–505, doi:10.1175/MWR-D-11-00068.1.

Galarneau, T. J., and C. A. Davis, 2013: Diagnosing forecast errors in tropical cyclone motion. *Mon. Wea. Rev.*, **141**, 405–430, doi:10.1175/MWR-D-12-00071.1.

Ge, X., T. Li, and M. Peng, 2013: Effects of vertical shears and midlevel dry air on tropical cyclone developments. *J. Atmos. Sci.*, **70**, 3859–3875, doi:10.1175/JAS-D-13-066.1.

Hanley, D., J. Molinari, and D. Keyser, 2001: A composite study of the interactions between tropical cyclones and upper-tropospheric troughs. *Mon. Wea. Rev.*, **129**, 2570–2584, doi:10.1175/1520-0493(2001)129<2570:ACSOTI>2.0.CO;2.

Jones, S. C., 1995: The evolution of vortices in vertical shear. I: Initially barotropic vortices. *Quart. J. Roy. Meteor. Soc.*, **121**, 821–851, doi:10.1002/qj.49712152406.

Molinari, J., and D. Vollaro, 1990: External influences on hurricane intensity. Part II: Vertical structure and response of the hurricane vortex. *J. Atmos. Sci.*, **47**, 1902–1918, doi:10.1175/1520-0469(1990)047<1902:EIOHIP>2.0.CO;2.

——, and ——, 2010: Rapid intensification of a sheared tropical storm. *Mon. Wea. Rev.*, **138**, 3869–3885, doi:10.1175/2010MWR3378.1.

——, P. Dodge, D. Vollaro, K. L. Corbosiero, and F. Marks, 2006: Mesoscale aspects of the downshear reformation of a tropical cyclone. *J. Atmos. Sci.*, **63**, 341–354, doi:10.1175/JAS3591.1.

——, J. Frank, and D. Vollaro, 2013: Convective bursts, downdraft cooling, and boundary layer recovery in a sheared tropical storm. *Mon. Wea. Rev.*, **141**, 1048–1060, doi:10.1175/MWR-D-12-00135.1.

Munsell, E. B., F. Zhang, and D. P. Stern, 2013: Predictability and dynamics of a nonintensifying tropical storm: Erika (2009). *J. Atmos. Sci.*, **70**, 2505–2524, doi:10.1175/JAS-D-12-0243.1.

Rappin, E. D., and D. S. Nolan, 2012: The effect of vertical shear orientation on tropical cyclogenesis. *Quart. J. Roy. Meteor. Soc.*, **138**, 1035–1054, doi:10.1002/qj.977.

Raymond, D. J., 1992: Nonlinear balance and potential-vorticity thinking at large Rossby number. *Quart. J. Roy. Meteor. Soc.*, **118**, 987–1015, doi:10.1002/qj.49711850708.

Reasor, P. D., and M. D. Eastin, 2012: Rapidly intensifying Hurricane Guillermo (1997). Part II: Resilience in shear. *Mon. Wea. Rev.*, **140**, 425–444, doi:10.1175/MWR-D-11-00080.1.

——, and M. T. Montgomery, 2015: Evaluation of a heuristic model for tropical cyclone resilience. *J. Atmos. Sci.*, **72**, 1765–1782, doi:10.1175/JAS-D-14-0318.1.

——, ——, and L. D. Grasso, 2004: A new look at the problem of tropical cyclones in vertical shear flow: Vortex resiliency. *J. Atmos. Sci.*, **61**, 3–22, doi:10.1175/1520-0469(2004)061<0003:ANLATP>2.0.CO;2.

——, R. Rogers, and S. Lorsolo, 2013: Environmental flow impacts on tropical cyclone structure diagnosed from airborne Doppler radar composites. *Mon. Wea. Rev.*, **141**, 2949–2969, doi:10.1175/MWR-D-12-00334.1.

Riemer, M., M. T. Montgomery, and M. E. Nicholls, 2010: A new paradigm for intensity modification of tropical cyclones: Thermodynamic impact of vertical wind shear on the inflow layer. *Atmos. Chem. Phys.*, **10**, 3163–3188, doi:10.5194/acp-10-3163-2010.

——, ——, and ——, 2013: Further examination of the thermodynamic modification of the inflow layer of tropical cyclones by vertical wind shear. *Atmos. Chem. Phys.*, **13**, 327–346, doi:10.5194/acp-13-327-2013.

Rios-Berrios, R., R. D. Torn, and C. A. Davis, 2016: An ensemble approach to investigate tropical cyclone intensification in sheared environments. Part I: Katia (2011). *J. Atmos. Sci.*, **73**, 71–93, doi:10.1175/JAS-D-15-0052.1.

Rogers, R., P. Reasor, and S. Lorsolo, 2013: Airborne Doppler observations of the inner-core structural differences between intensifying and steady-state tropical cyclones. *Mon. Wea. Rev.*, **141**, 2970–2991, doi:10.1175/MWR-D-12-00357.1.

Shu, S., F. Zhang, J. Ming, and Y. Wang, 2014: Environmental influences on the intensity changes of tropical cyclones over the western North Pacific. *Atmos. Chem. Phys.*, **14**, 6329–6342, doi:10.5194/acp-14-6329-2014.

Tang, B., and K. Emanuel, 2012: Sensitivity of tropical cyclone intensity to ventilation in an axisymmetric model. *J. Atmos. Sci.*, **69**, 2394–2413, doi:10.1175/JAS-D-11-0232.1.

Tao, D., and F. Zhang, 2014: Effect of environmental shear, sea-surface temperature, and ambient moisture on the formation and predictability of tropical cyclones: An ensemble-mean perspective. *J. Adv. Model. Earth Syst.*, **6**, 384–404, doi:10.1002/2014MS000314.

Wang, Y., Y. Rao, Z.-M. Tan, and D. Schnemann, 2015: A statistical analysis of the effects of vertical wind shear on tropical cyclone intensity change over the western North Pacific. *Mon. Wea. Rev.*, **143**, 3434–3453, doi:10.1175/MWR-D-15-0049.1.

Wong, M. L. M., and J. C. L. Chan, 2004: Tropical cyclone intensity in vertical wind shear. *J. Atmos. Sci.*, **61**, 1859–1876, doi:10.1175/1520-0469(2004)061<1859:TCIIVW>2.0.CO;2.

Zhang, F., and D. Tao, 2013: Effects of vertical wind shear on the predictability of tropical cyclones. *J. Atmos. Sci.*, **70**, 975–983, doi:10.1175/JAS-D-12-0133.1.